Realistic glottal motion and airflow rate during human breathing

Adam Scheinherr, Lucie Bailly, Olivier Boiron, Aude Lagier, Thierry Legou,
Marine Pichelin, Georges Caillibotte, Antoine Giovanni

HAL Id: hal-01348660

https://hal.science/hal-01348660

Submitted on 10 May 2023

Realistic glottal motion and airflow rate during human breathing

Adam Scheinherr [a,*], Lucie Bailly [a,b,c], Olivier Boiron [a], Aude Lagier [d,e], Thierry Legou [d],
Marine Pichelin [f], Georges Caillibotte [f], Antoine Giovanni [d,e]

a CNRS, Aix Marseille Université, Centrale Marseille, IRPHE UMR 7342, 13384, Marseille, France
b CNRS,3SR,F-38000Grenoble,France
c Univ. Grenoble Alpes, 3SR, F-38000, Grenoble, France
d CNRS, Aix Marseille Université, LPL UMR 7309, 13100, Aix-en-Provence, France
e APHM, ENT Department, La Timone Hospital, 13385, Marseille, France
f Air Liquide Healthcare, CRCD, 78354, Jouy en Josas, France

The glottal geometry is a key factor in the aerosol delivery efficiency for treatment of lung diseases. However, while glottal vibrations were extensively studied during human phonation, the realistic glottal motion during breathing is poorly understood. Therefore, most current studies assume an idealized steady glottis in the context of respiratory dynamics, and thus neglect the flow unsteadiness related to this motion. This is particularly important to assess the aerosol transport mechanisms in upper airways.

This article presents a clinical study conducted on 20 volunteers, to examine the realistic glottal motion during several breathing tasks. Nasofibroscopy was used to investigate the glottal geometrical variations simultaneously with accurate airflow rate measurements. In total, 144 breathing sequences of 30s were recorded.

Regarding the whole database, two cases of glottal time-variations were found: "static" or "dynamic" ones. Typically, the peak value of glottal area during slow breathing narrowed from 217 ± 54 mm^2 (mean $\pm$ STD) during inspiration, to 178 ± 35 mm^2 during expiration. Considering flow unsteadiness, it is shown that the harmonic approximation of the airflow rate underevaluates the inertial effects as compared to realistic patterns, especially at the onset of the breathing cycle. These measurements provide input data to conduct realistic numerical simulations of laryngeal airflow and particle deposition.

1. INTRODUCTION

Inhaled therapies play a major role in the treatment of lung diseases like asthma or chronic obstructive pulmonary diseases. Basic advantage of aerosol therapy lies in the direct delivery of high local concentrations of the drug to the site of action [1]. However, characteristics of inhaled particles, airways morphology, carrier gas and flow properties can largely influence the transport mechanisms and treatment efficiency [2–5]. Particularly, the upper airways (UA) anatomic arrangement can act as an unwanted filter, which limits the amount of drug delivered to the lungs. Recent clinical experiments have been conducted to quantify the distribution of radiolabeled aerosols in the human airways using combined single photon emission computed tomography (SPECT) and X-ray computer tomography (CT) [6,7]. It was shown that particle deposition in

extra-thoracic region can reach as much as 40% of the inhaled mass in the worst cases.

More specifically, within the larynx, the glottis (the space between vocal folds) narrows the airways to a minimal transition cross-section. Therefore its geometrical variations can affect breathing flow resistance [8–11]. This anatomical singularity yields to a complex jet-like glottal airflow, important recirculation zones and a locally turbulent behavior [12–19], which can be determinant on particle deposition by inertial impaction [3,20,21]. Regarding the glottal geometry's impact on the tracheal flow during breathing, a devoted description has been given by Brouns et al. [18,19]. This numerical study demonstrates the effect of the glottal size and shape on the overall fluid dynamics behavior, using a 3D idealized model of upper airways comprising a static glottis of parametrical aperture. This typical flow alteration can yield to the rise of the tracheal deposition of nano- and micrometer particles by factors ranging from 2 to 10 [20]. However, as pointed out in Brouns et al. [18], there is a current need for rendering the design of future upper airway models even more realistic, including glottal shape, area and kinematics in correlation with a given inlet inhalation flow rate. Thus, the knowledge of realistic

---

* Corresponding author. Tel.: 33 4 13 55 20 51; fax: 33 4 13 55 20 01.
E-mail address: Scheinherr@irphe.univ-mrs.fr, adam.scheinherr@email.cz
(A. Scheinherr).

Physical characteristics of the subjects. (* subject finished only *slow breathing* tasks; [†] subject finished only Eup_f task).

Females			Males		
Subject	Age [year]	BMI [kg.m^{-2}]	Subject	Age [year]	BMI [kg.m^{-2}]
F01	27	21.0	M01	25	21.2
F02	24	20.0	M02	26	24.3
F03	24	17.3	M03	24	22.5
F04	22	21.1	M04	28	20.3
F05	25	21.5	M05	25	23.1
F06	23	22.5	M06	27	23.0
F07	25	19.9	M07[†]	26	20.5
F08	23	23.4	M08	26	21.0
F09*	23	17.6	M09	26	20.1
F10	26	21.3	M10	27	21.8
Mean	**24.2**	**20.6**	**Mean**	**26**	**21.8**
SD	1.5	1.9	SD	1.2	1.4

glottal motion during human breathing will enable to further assess the filtration efficiency of the upper airways.

In this context, the purpose of the present study is to determine the glottal motion during several oral breathing tasks, and to investigate the correlation between this motion and the measured breathing flow rates. The first *in vivo* observation of the glottal motion dates back to the 19th century, with Garcia's laryngeal mirror [22]. Since the 1980s, advances in the medical equipment have allowed a refined exploration of the vocal-fold dynamics using laryngoscopy [9,10], high-speed cinematography [23,24], videokymography [25], electroglottography [26] or photoglottography [27]. These experimental techniques were extensively used to characterize the vocal-fold vibrations during human phonation (e.g. see a review by Ziethe et al. [28]). By contrast, however, the glottal variations during different human breathing regimes have been barely investigated so far. Despite a few reference studies [9,10,29], the relationship between the glottal area and the inhaled airflow rate is still poorly understood. In the present work, a clinical database comprising 8 breathing tasks recorded on 20 healthy subjects is presented. The physiological mechanisms of the respiratory cycles were observed using video-recording of laryngofiberscopic examinations, and synchronized oral airflow measurements. A quantitative characterization of glottal motion was derived from the processing of the recorded laryngeal images. The impact of the glottal motion on flow parameters is discussed as a function of breathing task and subject gender.

2. Materials and methods

The recording sessions took place at the Otolaryngology Department of the La Timone Adults Hospital (APHM, Marseille, France). In the following, the "realistic glottal motion" is defined by the 2D time-variations of the space area separating both free edges of the vocal folds, as observed *in vivo* on their superior transversal plane.

2.1. In vivo recordings

2.1.1. Subjects
From 20 healthy volunteers (10 females Fi, and 10 males Mi, i ∈ [01, 02, … , 10]) were obtained informed consents for the study. All subjects were non-smokers, without any professional sportive activity, any previous laryngeal or respiratory disorders, aging between 22 and 28 years. Table 1 lists the subject's age and body mass index (BMI).

2.1.2. Breathing tasks and database
Each subject was asked to produce eight 30s-tasks of slow or rapid breathing, described as follows:
Slow breathing tasks—below 20 cycles.min^{-1}:

(i) **Eup_f**: task of free *eupnea* (quiet breathing)
(ii) Repetition of **Eup_f**
(iii) **Eup_{15}**: task of *eupnea* with a controlled breathing frequency at 15 cycles.min^{-1}.
(iv) **Hyper_f**: task of free *hyperpnea* (deep breathing with maximal respiratory volume)

Rapid breathing tasks: above 20 cycles.min^{-1}:

(v) **Tachyp_{30}**: task of *tachypnea* with a controlled breathing frequency at 30 cycles.min^{-1}.
(vi) **Tachyp_{60}**: task of *tachypnea* with a controlled breathing frequency at 60 cycles.min^{-1}.
(vii) **Tachyp_{90}**: task of *tachypnea* with a controlled breathing frequency at 90 cycles.min^{-1}.

Specific inhalation task:

(viii) **Aerosol**: task mimicking the breathing gesture typically performed when using a dry powder inhaler to deliver medication (quick and deep inspiration followed by slow expiration).

For all tasks, the subject's nose was closed to ensure that the subject breathed only through his mouth. Note that both tasks of *free eupnea* (**Eup_f**) were intentionally presented to the subject as a phase of acquisition trials. This aimed to prepare him before the recording of the controlled tasks, which were described as the target of the study. Thereby, by reducing the effect of a motor control focused on the respiration, tasks (i) and (ii) were acquired in condition of spontaneous breathing. By contrast, the other tasks corresponded to cases of controlled breathing, for which the subjects were asked to synchronize their breathing frequency with a metronome projected on an instruction computer. These tasks intended to explore the extent of glottal motion and breathing capacity in specific respiratory contexts. In the end, 18 volunteers only (9 females and 9 males) successfully performed the entire protocol, thus yielding to a database comprising 144 sequences of 30s.

2.1.3. Measurements
All measurements were done in the seated posture. The glottis was observed using a flexible nasofiberscope equipped with a PAL camera (Storz endovision XL 202800) and a continuous cold light source. Laryngeal images were captured at a frequency of 25 Hz (768 × 288 pixels). The airflow rate was simultaneously registered by means of a pneumotachograph placed at the mouth, the EVA2^{TM} system (S.Q.Lab, www.sglab.fr) [30]. It consists of a two-grid flowmeter characterized by a small dead volume, specific linearized response for the inhaled and exhaled flow, and an accuracy of 1 cm^{3}s^{-1}. The sampling frequency of the flow rate signal was 6250 Hz. A trigger generated by an acquisition tool developed in NI LabWindows^{TM}/CVI was used to synchronize the recordings of laryngeal images and flow rate signal. Note that for several subjects, a local anesthetic (Lidocaine Aguettant 5%) was sprayed in the naris before the fiberscope introduction, so as to provide a better comfort during the invasive examination. Ambient temperature T_a [K] was also measured.

2.2. Data processing

All data was processed using Matlab®. Any point in the upper airways was located by the (x, y, z) coordinates as introduced in Fig. 1.

2.2.1. Airflow rate
Within each recorded 30s-sequence, every respiratory cycle was detected on the airflow signal, Q, using a zero-tracking method. Conventionally, positive and negative flow rate values correspond to inspiration and expiration, respectively. A BTPS correction (Body Temperature Pressure Saturated) was applied to convert the flow measured at ambient conditions to the thermodynamic conditions
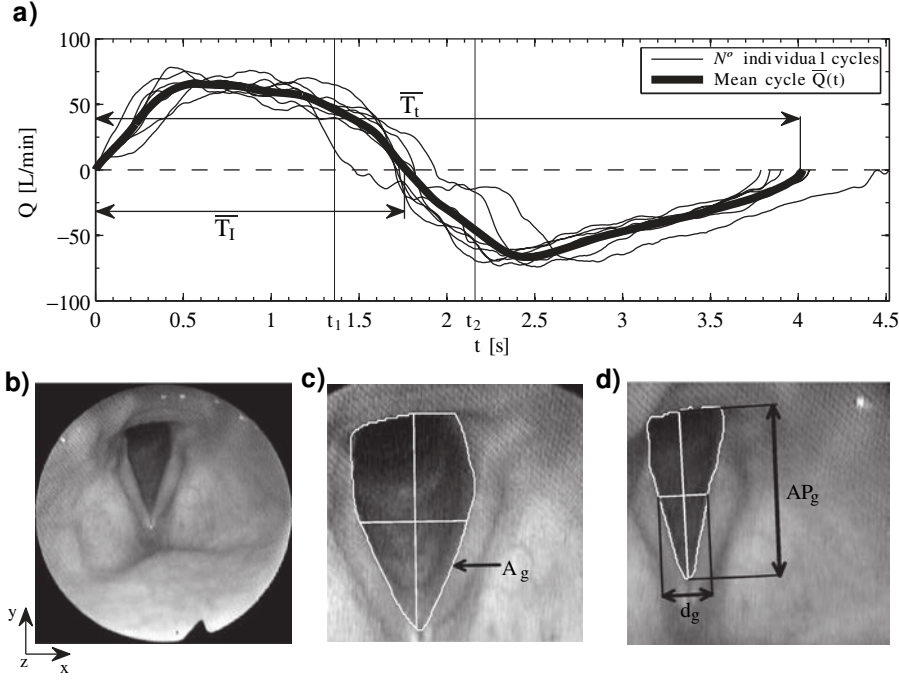
Fig. 1. (a) Superposed individual breathing cycles $Q(t)$ (subject M01, task **Eup$_{15}$**) and resulting mean breathing cycle in function of time t [s]. (b) Example of laryngoscopic area. Corresponding contour of glottal area A_g, antero-posterior diameter AP_g and glottal width d_g at the time of maximum opening t_1 (c) and at time of minimum opening t_2 (d).

expected within the extrathoracic region [31]. For each sequence, the Q-zero axis was updated so that $\overline{V_E} = C_c \overline{V_I}$, where $\overline{V_E}$ [L] is the average expiratory volume, $\overline{V_I}$ [L] is the average inspiratory volume and C_c [–] denotes for the BTPS conversion coefficient, $C_c = \frac{310}{T_a} \frac{P_a - P_{WS}}{P_a - 6.26}$. Pressure P_{WS} [kPa] is the saturation pressure of water vapor at ambient temperature T_a [K] and ambient pressure P_a [kPa]. C_c was quasi-constant over the whole database, equal to 1.07 (see Table 2, column #6). Each corrected sequence was averaged into one mean flow rate $\overline{Q}(t) = \frac{1}{N^\circ} \sum_{j=1}^{N^\circ} Q(t + j\overline{T_t})$ [L.min^{-1}], where N° stands for the number of breathing cycles with average period $\overline{T_t}$ [s] as illustrated in Fig. 1a.

2.2.2. Glottal motion detection

This procedure was limited to the analysis of two major tasks, **Eup$_{15}$** and **Tachyp$_{30}$**, altogether representing *slow* and *rapid breathing tasks* respectively. At first, breathing cycles, with hidden glottis aperture (by epiglottis or arytenoid cartilages) were removed from the video processing. Finally, about 126 (252) respiratory cycles out of 149 (291) were associated to task **Eup$_{15}$** (**Tachyp$_{30}$**). For these retained sequences, the glottal motion was extracted from each laryngoscopic image k taken at shot-instant t_k as follows: (i) correction of x- and y-motions of the fiberscope and focus on a region of interest using a customized cross-correlation technique; (ii) smoothing of the resized image using a Gaussian bandpass filtering; (iii) detection of the glottal area $A_g(t_k)$ contours applying a geodesic active contour-based method [32], as shown in Fig. 1c; (iv) determination of antero-posterior diameter $AP_g(t_k)$ (see Fig. 1d): at first 2 points were detected on left and right vocal-fold contour to identify the left and right glottal border lines; then, from the intersection of those border lines was derived a centerline; at last AP_g was defined by the 2 cross points of the centerline with the vocal-fold contour; (v) determination of glottal width $d_g(t_k)$ (see Fig. 1d), as a perpendicular line to AP_g at its mid-level; (vi) correction of vertical movement of the larynx and z-motion of the fiberscope by assuming AP_g as a geometrical invariant during breathing [33]; (vii) finally, conversion of the measured data from pixels to millimeters, assuming $AP_g = 22.1$ mm for males and 17.6 mm for females [34]. Note that the relevance of these latter values was preliminary checked using other means of clinical investigation allowing an easier spatial calibration, such as the high resolution computed tomographic scans recorded by Fleming et al. [6]. In particular, a typical value of 22 mm was confirmed by this technique in the case of a male adult.

2.2.3. Methodology accuracy

The measurement of the distance between the camera extremity and the glottal plane would enable direct dimensions conversion from pixels to millimeters. However, touching the glottal plane was not allowed as it could cause laryngospasm. Therefore, we chose the hypothesis of AP_g being a geometrical invariant [33] as an alternative to convert our pixels measurements. This assumption was previously applied by several authors [10,35,36]. The accuracy of the protocol was tested by recording a printed glottal image while simulating motions of the camera along x-, y- and z-directions. The glottal dimensions were detected with an average error smaller than 5%. Nevertheless, depending on the recorded laryngoscopic image quality (e.g. variable light contrast), the maximal error reached by the detection procedure was assessed at 10%.

3. RESULTS

In the followings, if X is a function of time t, X_{max} refers to the maximum value of X over duration t.

3.1. Airflow-rate pattern

For each task and gender of the database, Table 2 summarizes the measured primary respiratory variables $\overline{T_t}$ [s], mean inspiration airflow rate peak $\overline{Q_I^{max}}$ [L.min^{-1}] and inspired volume $\overline{V_I}$ [L]. Derived ratios $\overline{T_t}/\overline{T_I}$ ($\overline{T_I}$ [s] being the mean inspiration period, see Fig. 1a), $\overline{Q_I^{max}}/\overline{Q_E^{max}}$ ($\overline{Q_E^{max}}$ [L.min^{-1}] being the mean expiration airflow rate peak), and the BTPS correction factor C_c are also reported, as well as the number of processed breathing cycles N°. Figs. 2 and 3 present the corresponding normalized mean flow-rates $\overline{Q}/\overline{Q^{max}}$ as a function of ωt [rad], where ω is the pulsation of the average cycle defined as $\omega = 2\pi /\overline{T_t}$. The flow-rates obtained for the *slow breathing tasks* (i) to

Table 2

Measured airflow rate parameters in function of gender and breathing task (see chapter Airflow rate pattern in Results). Gray lines are the tasks further treated for the glottal motion analysis.

Males

Task	$\bar{T}_t$ [s] mean SD	range	$\bar{T}_t/\bar{T}_I$ [-] mean SD	range	$\bar{Q}_I^{max}$ [Lmin⁻¹] mean SD	range	$\bar{Q}_I^{max}/\bar{Q}_E^{max}$ [-] mean SD	$\bar{V}_I$ [L] mean SD	range	C_c [-] mean SD	N^o sum
Eup$_f$	**2,96** 0,78	1.5–5.8	**2,10** 0,16	1.43–3.45	**42,7** 11,7	11.5–84.8	**0,88** 0,19	**0,66** 0,15	0.12–1.42	**1,08** 0,05	256
Eup$_{15}$	**3,99** 0,03	3.7–4.5	**2,26** 0,21	1.82–3.04	**49,3** 14,2	30.8–86.6	**1,11** 0,17	**0,98** 0,34	0.52–2.11	**1,07** 0,01	68
Tachyp$_{30}$	**2,00** 0,01	1.8–2.4	**2,13** 0,16	1.69–2.55	**72,4** 28,0	37.6–167.6	**0,98** 0,16	**0,81** 0.36	0.42–1.99	**1,07** 0,01	145
Tachyp$_{60}$	**1,02** 0,06	0.8–1.3	**2,10** 0,13	1.72–2.99	**93,2** 51,1	49.3–271.5	**1,02** 0,15	**0,55** 0,32	0.20–1.66	**1,07** 0,01	327
Tachyp$_{90}$	**0,75** 0,02	0.6–0.9	**2,11** 0,18	1.70–3.02	**102,6** 63,8	45.9–343.8	**1,02** 0,16	**0,45** 0,29	0.18–1.47	**1,07** 0,01	393
Hyper$_f$	**7,39** 2,50	3.5–12	**2,20** 0,19	1.73–2.67	**125,7** 62,0	56.1–329.4	**1,11** 0,30	**3,82** 1.44	2.38–8.90	**1,07** 0,01	38
Aerosol	**3,29** 1,15	1.4–5.8	**3,55** 0,92	2.09–6.82	**263,1** 126,3	118.5–586.7	**3,58** 1,09	**1,83** 0,72	1.19–3.96	**1,07** 0,01	38

Females

Task	$\bar{T}_t$ [s] mean SD	range	$\bar{T}_t/\bar{T}_I$ [-] mean SD	range	$\bar{Q}_I^{max}$ [Lmin⁻¹] mean SD	range	$\bar{Q}_I^{max}/\bar{Q}_E^{max}$ [-] mean SD	$\bar{V}_I$ [L] mean SD	range	C_c [-] mean SD	N^o sum
Eup$_f$	**4,00** 1,04	2.2–3.5	**2,36** 0,22	1.56–2.36	**32,2** 7,2	15.5–32.0	**1,12** 0,17	**0,64** 0,18	0.29–0.56	**1,07** 0,02	217
Eup$_{15}$	**3,99** 0,03	3.6–4.1	**2,21** 0,10	1.94–2.15	**42,9** 8,4	23.4–35.5	**1,06** 0,09	**0,94** 0,23	0.38–0.71	**1,07** 0,02	81
Tachyp$_{30}$	**1,99** 0,00	1.8–2.1	**2,12** 0,12	1.81–2.55	**50,9** 9,1	30.0–75.8	**0,99** 0,11	**0,61** 0,13	0.27–0.98	**1,07** 0,02	146
Tachyp$_{60}$	**1,00** 0,00	0.8–1.2	**2,10** 0,11	1.59–2.84	**60,0** 13,2	31.0–97.9	**1,04** 0,12	**0,36** 0,08	0.14–0.64	**1,08** 0,01	332
Tachyp$_{90}$	**0,73** 0,04	0.4–1.1	**2,10** 0,15	1.63–3.55	**59,9** 15,4	33.8–99.2	**1,03** 0,16	**0,26** 0,08	0.11–0.60	**1,07** 0,01	476
Hyper$_f$	**8,00** 2,53	5.1–13.4	**2,32** 0,19	1.80–2.77	**75,3** 22,2	46.4–112.6	**1,11** 0,09	**2,54** 0,57	1.35–3.70	**1,07** 0,01	43
Aerosol	**3,19** 1,05	1.9–5.5	**4,74** 1,92	2.49–13.04	**161,6** 35,9	89.3–252.6	**3,10** 0,92	**1,12** 0,24	0.57–1.84	**1,07** 0,01	46
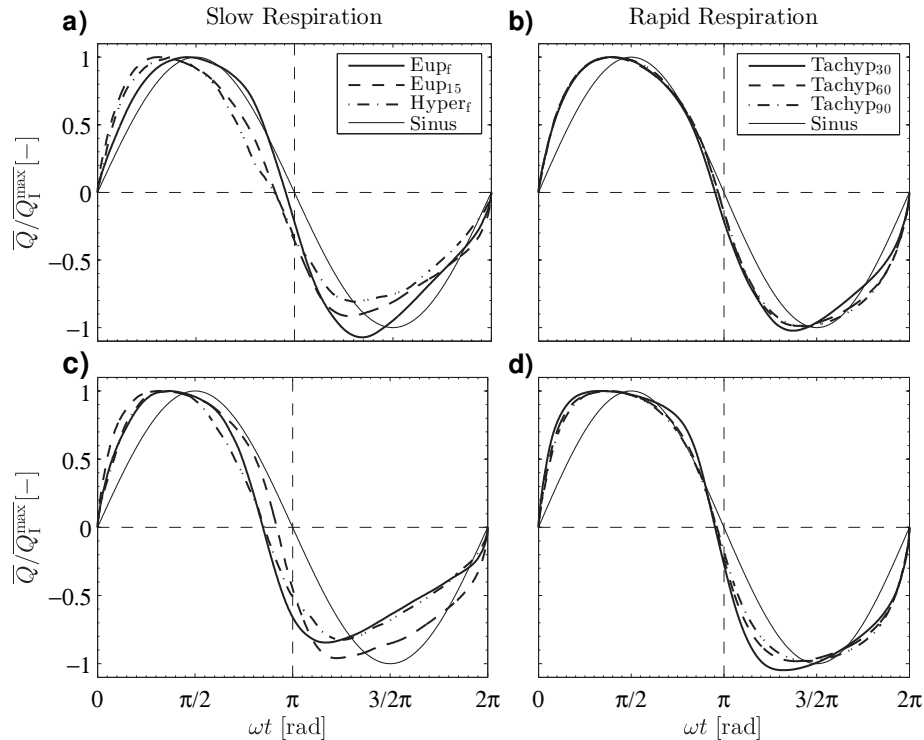
Fig. 2. Normalized mean flow rates $\overline{Q}/\overline{Q}_I^{max}$ as function of ωt [rad] for *slow breathing* tasks (**Eup$_f$, Eup$_{15}$, Hyper$_f$**) (Panels a and c for males and females, respectively) and *rapid breathing* tasks (**Tachyp$_{30}$, Tachyp$_{60}$, Tachyp$_{90}$**) (Panels b and d for males and females, respectively).
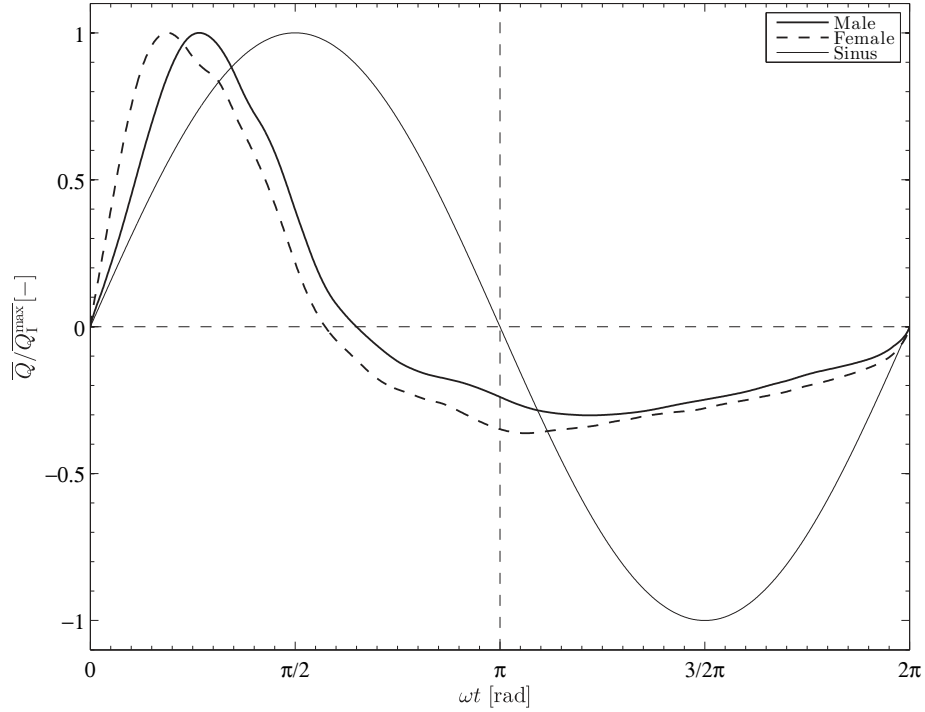
Fig. 3. Normalized mean flow rates $\overline{Q}/\overline{Q_I^{\max}}$ as function of ωt [rad] for the *specific inhalation task* **Aerosol** and males and females.

(iv) (see Figs. 2a and 2c for males and females respectively), and *rapid breathing tasks* (v) to (vii) (see Figs. 2b and 2d) are displayed. The flow-rate obtained for the *specific inhalation task* (viii) is plotted in Fig. 3.

3.1.1. General features

For each case, the measured airflow pattern was confronted to the sinusoidal evolution $\sin(\omega t)$, commonly used as an idealized breathing pattern [4,27]. For *slow* and *rapid breathing* tasks, Fig. 2 shows that the quasi-sinusoidal approximation can be *a priori* usable as a whole. Yet, several discrepancies can be highlighted. First, the Euclidean distance between measurements and this harmonic signal (noted $\varepsilon_i[-]$ at instant t_i) is smaller for male than female subjects ($\varepsilon = 5.4$ versus 6.9, mean value over breathing cycle). Furthermore, the approximation is closer to measurements during inspiration ($\varepsilon = 5.0$) than during expiration phase ($\varepsilon = 7.3$). Note that smallest distances ε_i were found during inspiratory phases of tasks **Eup$_f$**, **Tachyp$_{30}$**, **Tachyp$_{60}$** and **Tachyp$_{90}$** ($\varepsilon \cong 3.8$), whereas largest ε_i were found for the **Aerosol** task (9.1 and 17.1 for inspiration and expiration, respectively). Now, whatever the task, a phase difference in maximal flow rate occurrences has been measured between sinusoid and realistic patterns. We found a phase angle smaller for male subjects than female (27.1° in comparison with 36.0°), and smaller for inspiration than for expiration (26.8° in comparison with 36.3°). Over the whole database, the smallest phase difference was found for task **Eup$_f$** (8.0° for males, inspiration). Considering males and females together, over the whole cycle a phase difference around 21.1° was measured for tasks **Eup$_f$**, **Tachyp$_{30}$**, **Tachyp$_{60}$**, **Tachyp$_{90}$** and **Hyper$_f$**, and around 39.3° for **Eup$_{15}$** task. At last, for both genders, the phase difference for **Aerosol** task reached the highest values (up to 79°). Thus, the sinusoidal hypothesis is no more valuable in case of *specific inhalation task* (Fig. 3).

3.1.2. Breathing frequency

From $\overline{T_t}$ in Table 2 can be deduced that spontaneous *slow breathing* (**Eup$_f$**) was achieved at a mean frequency of 20 cycles.min^{-1} for males and 15 cycles.min^{-1} for females. The measured frequencies of tasks **Eup$_{15}$**, **Tachyp$_{30}$** and **Tachyp$_{60}$** correspond to the target values,

which validates the protocol for this range of breathing rates. Note that the target value chosen for task **Tachyp$_{90}$** (90 cycles.min^{-1}) was excessively high for most of the subjects, who worked out with a breathing frequency around 80 cycles.min^{-1} instead. All the tasks were performed so that in average $\overline{T_t}/\overline{T_I} > 2$, thereby yielding to an inspiratory duration shorter than the expiratory one, as found in previous studies made on healthy subjects [37]. In particular, in Proctor & Hardy [38], a ratio $\overline{T_t}/\overline{T_I}$ was measured in the range 1.57–2.9 during quiet breathing (including patients with pulmonary disease), versus 1.43–3.45 in our case (mean value 2.10 and 2.36, for male and female groups respectively).

3.1.3. Breathing amplitude

Values of the flow-rate maximal amplitudes $\overline{Q^{\max}}$ are very different inter-tasks and inter-subjects, as detailed in Table 2. Over the whole database, the amplitudes are 30% higher for male than for female subjects. During spontaneous breathing, typical peak values ranged between 29 L.min^{-1} and 68 L.min^{-1}, with a mean value of 43 L.min^{-1} for males, and 32 L.min^{-1} for females. These results are in line with previous studies (see range of values from 13 L.min^{-1} to 78 L.min^{-1} in Proctor & Hardy [38]).

3.2. Glottal motion

Table 3 summarizes the primary glottal dimensional parameters ($\overline{A_g}$, $\overline{A_g^I}$ and $\overline{A_g^{I\,\max}}$) measured during *slow breathing* (**Eup$_{15}$**) and *rapid breathing* (**Tachyp$_{30}$**). Area $\overline{A_g}$ is the mean glottal area obtained over the average cycle $\overline{Q}$; $\overline{A_g^I}$ is the mean glottal area obtained during inspiration (resp. $\overline{A_g^E}$ during expiration), and $\overline{A_g^{I\,\max}}$ is the peak value of $\overline{A_g^I}$ area (resp. $\overline{A_g^{E\,\min}}$ is the minimum value of $\overline{A_g^E}$). The derived ratios $\overline{A_g^I}/\overline{A_g^E}$ (resp. $\overline{A_g^{I\,\max}}/\overline{A_g^{E\,\min}}$), representing the ratio of the mean (resp. peak) $\overline{A_g}$ amplitude during inspiratory and expiratory phases, are also reported. The variations of $\overline{A_g}$ in function of $\overline{Q}$ for all subjects are shown in Figs. 4 and 5, for *slow* and *rapid breathing* respectively.

5

Table 3
Measured glottal dimensions parameters in function of gender, group of subjects and breathing rate. Gray lines are the groups for which a time-varying glottal area was detected during the average breathing cycle.

Group	$\overline{A_g}$ [mm²]	$\overline{A_g^I}$ [mm²]		$\overline{A_g^{I\,max}}$ [mm²]		$\overline{A_g^I}/\overline{A_g^E}$ [−]		$\overline{A_g^{I\,max}}/\overline{A_g^{E\,max}}$ [−]	N°
	Mean SD	Mean SD	Range	Mean SD	Range	Mean SD	Range	Mean SD	Sum
Slow Breathing–Eup$_{15}$									
M-1st group	**187** 4	**191** 9	185–198	**194** 15	200–221	**1.03** 0.05	1.01–1.08	**1.08** 0.07	14
F-1st group	**186** 27	**187** 29	150–241	**189** 34	159–362	**1.01** 0.03	0.96–1.04	**1.03** 0.05	47
M-2nd group	**199** 48	**214** 49	154–299	**224** 59	194–348	**1.15** 0.09	1.00–1.24	**1.26** 0.3	45
F-2nd group	**158** 13	**183** 26	157–210	**190** 32	181–246	**1.33** 0.24	1.20–1.61	**1.46** 0.35	20
M-all	**196** 42	**209** 44	154–299	**217** 54	194–348	**1.12** 0.10	1.00–1.24	**1.22** 0.31	59
F-all	**177** 27	**185** 27	150–241	**189** 32	165–274	**1.08** 0.20	0.96–1.61	**1.12** 0.32	67
Rapid Breathing–Tachyp$_{30}$									
M-1st group	**209** 6	**211** 9	200–217	**214** 10	222–241	**1.02** 0.04	0.97–1.05	**1.07** 0.05	41
F-1st group	**179** 14	**179** 12	162–196	**181** 18	176–230	**1.00** 0.04	0.94–1.05	**1.02** 0.05	98
M-2nd group	**214** 6	**227** 9	175–294	**236** 10	202–319	**1.11** 0.04	1.01–1.25	**1.24** 0.05	85
F-2nd group	**175** 57	**189** 47	157–223	**196** 54	176–252	**1.17** 0.18	1.08–1.34	**1.39** 0.08	28
M-all	**212** 39	**221** 41	175–294	**228** 43	202–319	**1.08** 0.09	0.97–1.25	**1.17** 0.22	126
F-all	**178** 23	**182** 20	157–223	**184** 25	176–252	**1.04** 0.11	0.94–1.34	**1.08** 0.22	126

3.2.1. General features

Every mean breathing cycle of the database is characterized by a mean ratio $\overline{A_g^I}/\overline{A_g^E}$ higher than 1. However, the time-variations of the detected glottal area demonstrate a substantial inter-subject variability. Within each gender and task category, the subjects were divided into two groups, represented in Table 3:

- The 1st group (labeled as "static") gathers the subjects with a quasi-constant glottal area detected during the average breathing cycle. This group is characterized by a mean glottal area variation smaller than 10%. The limit was assessed as the accuracy of the detection procedure. This "static" glottal evolution during breathing has been reported in Hyatt et al. [39] and in 1 subject out of 3 in Jackson et al. [8].
- The 2nd group (labeled as "dynamic") gathers the subjects with a time-varying glottal area during the average breathing cycle, so that the mean glottal area variation is higher than 10%. This group is characterized by a progressive glottal widening (resp. narrowing) during inspiration (resp. expiration), in agreement with previous reference studies [9,10,29]. In that case, the peak values reached during inspiration have been measured around 1.26 and 1.46 times higher than the minimum value achieved during expiration for males and females respectively. During *slow breathing*, the 2nd group is represented by 52.6% of subjects, against 44.4% during *rapid breathing*.

In the group as a whole, the average ratio $\overline{A_g^{I\,max}}/A_g^{E\,min}$ was ranging from 1.21 (subject F04) to 2.31 (subject M08). This ratio was evaluated at 1.8 in Brancatisano et al. [10] and between 1.16 and 1.54 in England et al. [29].

In our database, during *slow breathing*, the peak glottal area changes from $\overline{A_g^{I\,max}} = 217 \pm 54$ mm² (mean ± SD) during inspiration to $A_g^{E\,min} = 178 \pm 35$ mm² during expiration, for males. Similarly, for females, the peak glottal area changes from 189 ± 32 mm² dur-

ing inspiration to 168 ± 31 mm² during expiration. The mean value over the whole cycle, $\overline{A_g}$, was found at 196 ± 42 mm² for males, and 177 ± 27 mm² for females. The corresponding values for *tachypnea* breathing are stated in Table 3.

Another important feature can be highlighted from the present work. In average on our database, the measured glottal areas are much higher than those measured with equivalent method in other works [9,10]. Indeed, Baier et al. [9] measured a mean area $\overline{A_g}$ of 44 mm² and 48 mm² for 2 males. This area ranged from 43 mm² to 104 mm² for 4 females. Similarly, Brancatisano et al. [10] measured an area $\overline{A_g}$ of 98 mm² ($\overline{A_g^{I\,max}} = 126 \pm 8$ mm², 12 subjects, 2 females).

However, our results are in agreement with previous studies based on the acoustic reflection [40–42] or MRI technique [43]. In particular, D'Urzo et al. [40] used both acoustic reflection and CT methods to measure glottal area of 11 subjects. The results derived from both methods were similar. The values of A_g were measured at functional residual capacity, and varied between 40 and 290 mm² (mean value of 180 ± 80 mm²). Similarly, Martin et al. [42] measured an area of 170 mm² (114 subjects). Note that Rubinstein et al. [41] found a range of values between 144 and 211 mm² on 25 males and between 137 and 207 mm² on 19 females during *hyperpnea*.

A glottal narrowing during expiration was observed in all studies. This is supported by the activity of the thyroarytenoid muscle during expiration [44], which is an adductor muscle of the vocal folds.

3.2.2. Influence of subject gender

The influence of the subject gender on glottal variations during *slow breathing* is clearly highlighted in Fig. 4. In the upper panel (Fig. 4a and b), it is shown that 9 male subjects have much more representatives in the 2nd group "dynamic" (7/9) relative to the 1st group "static" (2/9). On the contrary, the lower panel (Fig. 4c and d) shows that 10 female subjects are gathered together in the 1st group "static" (7/10), compared with the 2nd group "dynamic" (3/10). These
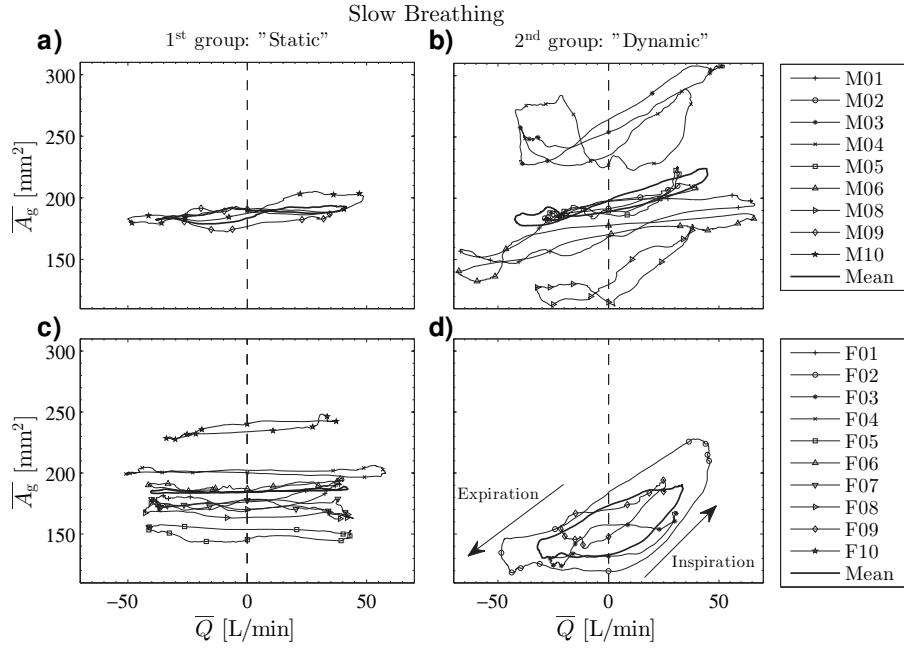
Fig. 4. Glottal area variations during *slow breathing*. Upper panels (a and b) are for male subjects, and lower panels (c and d) are for female subjects. Left panels (a and c) are dedicated to the 1st group (with "static" glottal movement) and right panels (b and d) are dedicated to the 2nd group (with "dynamic" glottal movement).
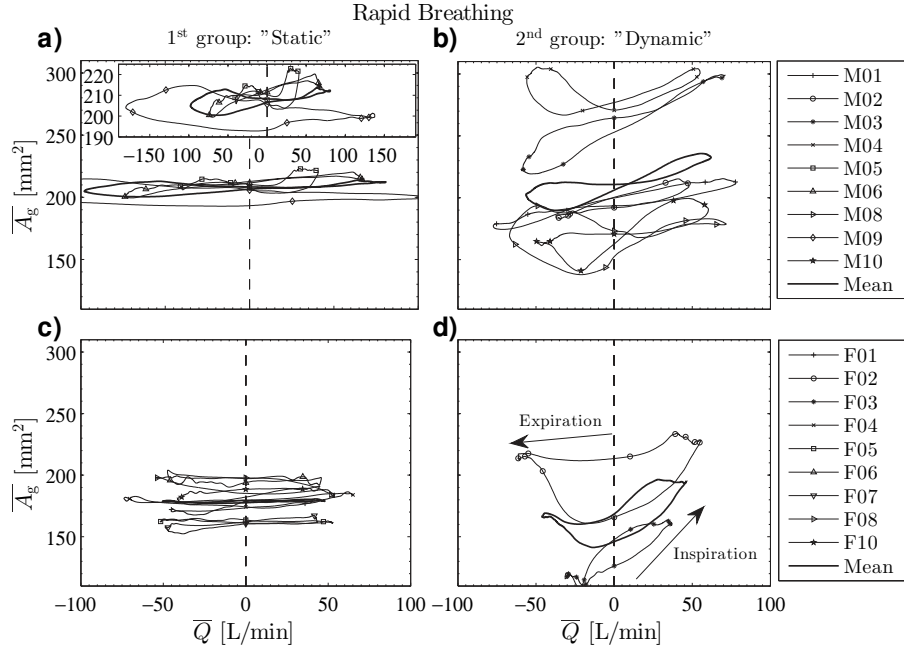

Fig. 5. Glottal area variations during *rapid breathing*. Upper panels (a and b) are for male subjects, and lower panels (c and d) are for female subjects. Left panels (a and c) are dedicated to the 1st group (with "static" glottal movement) and right panels (b and d) are dedicated to the 2nd group (with "dynamic" glottal movement). Panel a includes a detail of subject M08 for its high airflow rate variations.

trends are similar in *rapid breathing*, as displayed in Fig. 5 (6/9 males against 2/9 females only in 2nd group "dynamic").

Despite their minimal proportion within the 2nd group, females demonstrate glottal motion amplitudes larger than males. This result yields to higher ratios $\overline{A_g^I}/\overline{A_g^E}$ and $\overline{A_g^{I\max}}/\overline{A_g^{E\min}}$ for females, whatever the task (see Table 3, darkened rows). For both genders however, the mean loops $\overline{A_g}(\overline{Q})$ plotted in Fig. 4b and 4d do not exhibit ellipsoidal shapes, which would have been observed in case of sinusoidal dynamics. Instead, the shape-differences observed on the loops $\overline{A_g}(\overline{Q})$ of males and females mainly derive from the different time-variations

of the glottal area recorded during inspiration for both genders: a $\overline{A_g}$ plateau occurs during this phase for females, while a quasi-sinusoidal variation is measured for males (see Fig. 6). Note that during expiration, the glottal dynamics is similar for males and females: the glottis tends to stay opened in the narrowest posture (Fig. 6a and c).

3.2.3. Influence of breathing task

The comparison of the loops $\overline{A_g}(\overline{Q})$ given in Figs. 4 and 5 shows similar tendencies and orders of magnitude for *eupnea* and *tachypnea*.
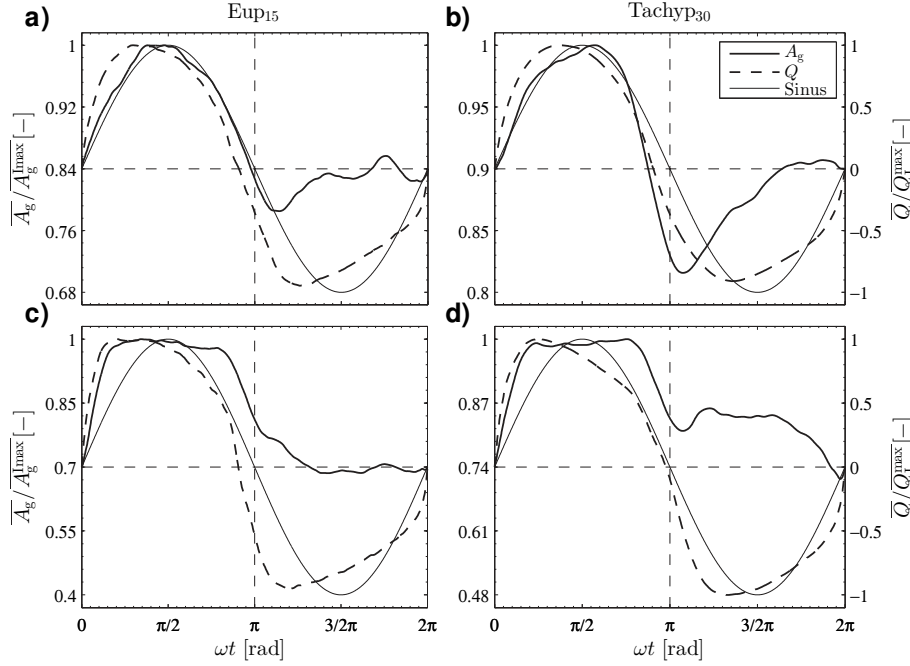
Fig. 6. Comparison of mean, normalized glottal area $\overline{A_g}/A_g^{l\,\max}$, mean, normalized flow rate $\overline{Q}/\overline{Q_l^{\max}}$, and sinusoidal pattern for males (panels a and b, tasks **Eup₁₅** and **Tachyp₃₀**, respectively) and for females (panels c and d, tasks **Eup₁₅** and **Tachyp₃₀**, respectively). Results are given for the subjects with "dynamic" glottal variations (2nd group).

From our results, the influence of the breathing task on glottal motion is far less emphasized than the one of the subject gender.

The glottal aperture is larger during the whole cycle for *tachypnea* than for *eupnea*. This is confirmed in Baier et al. [9], who measured larger glottal areas by both men and women during *tachypnea* than during *quiet breathing*.

3.3. Correlation between airflow-rate pattern and glottal motion

Fig. 6 shows the mean normalized glottal area dynamics $(\overline{A_g}/A_g^{l\,\max})$ in function of normalized time (ωt) for subjects classified within the 2nd group only. The 1st group is not presented here as the glottal dynamics is steady and the resulting normalized pattern would be a straight line close to 1. Upper (resp. lower) panels correspond to male subjects (resp. female). The mean normalized airflow-rate pattern $(\overline{Q}/\overline{Q_l^{\max}})$ is also displayed, to analyze the correlation between airflow-rate and glottal area time-variations. For all 2nd group subjects and tasks, the glottal widening starts with the onset of inspiration, whereas the glottal narrowing precedes the expiration phase. For males, the peak glottal area $\overline{A_g^{l\,\max}}$ is achieved after the peak inspiratory airflow $\overline{Q_l^{\max}}$, with a phase difference of 15.6°. For females, this delay is reduced and both peaks occur rather simultaneously. If the glottal motion seems related to the airflow dynamics during inspiratory phase, no correlation is brought out from the data registered during expiratory phase. Therefore, the same absolute airflow amplitude is associated with (at least) two different glottal openings.

4. Discussion

4.1. Toward the reasons for glottal motion and aerodynamics: an energy saving mechanism?

The respiratory-related glottal motion is generated by contractions of intralaryngeal muscles. The vocal-fold abductor (posterior cricoarytenoid muscle) dilates the glottis during inspiration by ab-

duction rotation of the arytenoid cartilages. The adductor muscles narrow the glottis during expiration by adduction-rotation of the arytenoid cartilages. There is general agreement that this controlled motion is carried out in order to (i) help the air intake during inspiration by glottis widening, which lowers the UA resistance to flow, and (ii) to slow down the passive expiratory airflow by glottis narrowing, which enables a control of the end-expiratory lung volume and prevents alveoli to collapse [10,45]. Note that several studies are dedicated to the restoration of an optimal laryngeal geometry after a surgical change of the vocal folds, which would minimize the airflow resistance in the UA [46,47].

Thus, the results obtained in our study on glottal motion and aerodynamics during breathing were further analyzed to interpret the data in terms of energy efficiency. To this end, the power dissipated by an airflow (volume airflow rate $Q^0(t)$) through a circular diaphragm ("glottis" of cross section area A_g^0) across a cylindrical tube ("trachea" of cross section area $A^t = AP_g$) was calculated in two comparative cases:

(i) a realistic case mimicking the measured *unsteady flow and glottal conditions*, where $Q^0(t) = \overline{Q}(t)$ and $A_g^0(t) = A_g(t)$.

(ii) an idealized case assuming *unsteady sinusoidal flow conditions* and *steady glottis*, where $Q^0(t) = \overline{Q_l^{\max}}\sin(\omega t)$ with $\overline{Q_l^{\max}} = \pi\,\overline{V_l}/\overline{T_t}$, and $A_g^0 = \overline{A_g}$.

Considering the air as an incompressible Newtonian gas with typical flow Reynolds number $Re < 10^5$, the power P_w [W] dissipated through a circular diaphragm is given by:

$$P_w = \Delta p \cdot Q^0 = \frac{1}{2}\rho\,U^2\lambda\,\left|\,Q^0\,\right|,$$

where Δp [Pa] is the pressure drop through the singularity, $\rho = 1.2$ [kg.m^{-3}] is the air density, $U = 2\overline{V_l}/(\overline{T_t}A_g^0)$ [m.s^{-1}] is the mean flow velocity during inspiration phase and λ [–], the singular head loss coefficient [48] calculated by $\lambda = (1 + 0.707\sqrt{1 - \frac{A_g^0}{A^t}} - \frac{A_g^0}{A^t})^2$. Fig. 7
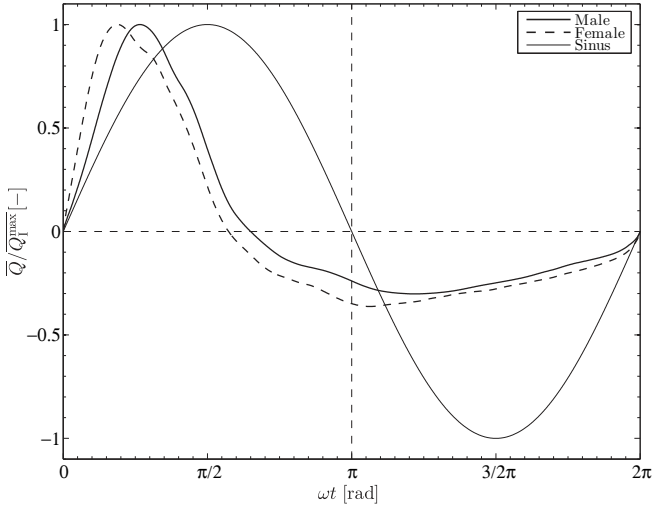
Fig. 7. Power P_w [mW] comparison of idealized and realistic case, obtained from the data registered for female and male subjects, in the illustrative case of *rapid breathing* (**Tachyp₃₀**).

Table 4
Energy loss E [mJ] within a circular diaphragm in two breathing modes: (i) mobile glottis, non-sinusoidal airflow and (ii) steady glottis, sinusoidal airflow.

Slow breathing–Eup₁₅		
Group	Realistic case (i)	Idealized case (ii)
Males	**2.73**	**2.84**
Females	**2.73**	**3.10**
Rapid breathing–Tachyp₃₀		
Males	**5.28**	**5.62**
Females	**2.86**	**3.28**

shows a comparison of the power P_w [mW] obtained from the data registered for female and male subjects, in the illustrative case of rapid breathing (**Tachyp₃₀**). Over the whole, it is interesting to note a substantial decrease of the power dissipated during the average breathing cycle in realistic case (i) as compared to idealized case (ii). The energy dissipated by head loss within the "glottal" diaphragm over a cycle, E [J], is defined as $E = \int_0^{\overline{T_t}} P_w dt$. Average values are presented in Table 4 in function of gender and breathing task. During *slow breathing* (resp. *rapid breathing*), the relative decrease between idealized and realistic cases equals 4% (resp. 6%) and 12% (resp. 13%) for males and females group respectively. Therefore, it is shown that the realistic breathing mode (mobile glottis, non-sinusoidal airflow rate) is an energy saving maneuver in comparison with an idealized mode (steady glottis, sinusoidal airflow rate).

4.2. Toward the aerodynamic impact of glottal motion

The database was also exploited to evaluate the impact of the measured glottal motion and airflow rates on characteristic flow parameters within the glottis, listed below:

- The maximum and mean flow velocity during inspiration, noted u_{max} and u_{mean};
- The local Reynolds numbers Re_{max} and Re_{mean} based on u_{max} and u_{mean}, respectively;
- The frequency parameter, given by $\alpha = R_h\sqrt{\omega/\upsilon}$, where $R_h = D_h/4$, D_h [m] being the hydraulic diameter and υ [m².s⁻¹] the air kinematic viscosity.

For each group, these parameters are function of the inspiratory volume $\overline{V_I}$, the breathing period T_t and the glottal cross-section area $\overline{A_g}(t)$. Table 5 presents the values obtained in conditions of *slow* and *rapid breathing* for males and females (based on data from Tables 2 and 3). The mean Reynolds numbers range between 1900 and 3100 (peak values below 5000), corresponding to moderate mean velocity values expected within the glottis (peak values between 4 and 6 m.s⁻¹). Low values of the frequency parameter (in the range 1.8–2.7) are indicators of a flow comprising notable viscous effects, and whose time duration of the boundary layer development is comparable to the breathing cycle period. These parameters provide information, which could be used as input data to conduct further realistic numerical simulations of laryngeal airflow.

Finally, it is important to note, that the fraction of aerosols deposited on the laryngeal walls is highly dependent on the Stokes number, defined as: $St = \rho_p d_p^2 u/(18\mu D_h)$, where ρ_p is the density of the particles, d_p the particle diameter, μ the air viscosity, u the air inlet velocity and D_h the glottal hydraulic diameter. Thus, the deposition dynamics in the larynx is likely to be altered (i) by unsteady flow velocity, as demonstrated in Jin et al. [49], in case of static wall conditions, but also (ii) by unsteady glottal dimensions during breathing. From this point of view, the clinical database reported in this study seems to us of primary interest to better evaluate the aerosol transport and deposition mechanisms in future work.

5. Conclusion

A clinical study was conducted to examine the glottal motion during eight breathing tasks by means of laryngofibroscopy and synchronized oral airflow measurements on 20 healthy non-smoking volunteers from 20 to 30 year-old. In total, 144 breathing sequences of 30s were recorded. Several results can be highlighted:

Two groups of subjects were identified: (i) a "static" group, gathering subjects with a constant glottal area detected during the average breathing cycle; (ii) a "dynamic" group, gathering subjects with a time-varying glottal area during the average breathing cycle. This latter group gathers 53% (respectively, 44%) of subjects during slow (respectively, rapid) breathing.

Table 5
Glottal airflow parameters derived from the present clinical database in function of gender and breathing rate.

| Flow parameter | Females | | Males | |
	Slow breathing	Rapid breathing	Slow breathing	Rapid breathing
u_{max} [m.s⁻¹]	4.17	5.41	3.93	5.99
u_{mean} [m.s⁻¹]	2.66	3.45	2.50	3.81
Re_{max} [–]	3069.2	4001.1	3087.9	4852.2
Re_{mean} [–]	1953.9	2547.2	1965.8	3089.0
α [–]	1.76	2.51	1.88	2.74
D_h [mm]	10.7	10.8	11.44	11.8

9

During "slow" breathing tasks, for males, the peak value of glottal area narrowed from 217 ± 54 mm^2 during inspiration, to 178 ± 35 mm^2 during expiration. For females, the peak glottal area changes from 189 ± 32 mm^2 during inspiration, to 168 ± 31 mm^2 during expiration. The mean value over the whole cycle was found at 196 ± 42 mm^2 for males, and 177 ± 27 mm^2 for females. These values are in agreement with previous studies based on acoustic reflection or MRI techniques. Yet, they are much higher than those previously determined by laryngofibroscopy, due to different spatial calibration.

A correlation motion related to the airflow dynamics was found during inspiratory phase, while no correlation was brought out from the data registered during expiratory phase.

Using a simple theoretical framework based on the power dissipated through a movable diaphragm, this study showed that the realistic breathing mode (mobile glottis, non-sinusoidal airflow rate) is an energy saving maneuver in comparison with an idealized mode (steady glottis, sinusoidal airflow rate).

Finally, this clinical database constitutes available input data which can be used to conduct further realistic numerical simulations of laryngeal airflow in realistic geometries of upper airways.

Funding

Conflicts of interest

None declared.

Ethical approval

Ethical approval was given by the Committee on the Protection of People (CPP) in Biomedical Research (CPP Sud Méditerranée I, n°2012-A01390-13).

Acknowledgement

References

[1] Khilnani GC, Banga A. Non-invasive ventilation in chronic obstructive pulmonary. Medicine (Baltimore) 2008:18.

[2] Finlay WH. The mechanics of inhaled pharmaceutical aerosols. London: Academic Press; 2001.

[3] Grgic B, Finlay WH, Heenan AF. Regional aerosol deposition and flow measurements in an idealized mouth and throat. J Aerosol Sci 2004;35:21–32.

[4] Sandeau J, Katz I, Fodil R, Louis B, Apiou-Sbirlea G, Caillibotte G, et al. CFD simulation of particle deposition in a reconstructed human oral extrathoracic airway for air and helium-oxygen mixtures. J Aerosol Sci 2010;41(3):281–94.

[5] Kleinstreuer C, Zhang Z. Airflow and particle transport in the human respiratory system. Annu Rev Fluid Mech 2010;42:301–34.

[6] Fleming J, Conway J, Majoral C, Tossici-Bolt L, Katz I, Caillibotte G, et al. The use of combined single photon emission computed tomography and x-ray computed tomography to assess the fate of inhaled aerosol. J Aerosol Med Pulm Drug Deliv 2011;24(1):49–60.

[7] Conway J, Fleming J, Majoral C, Katz I, Perchet D, Peebles C, et al. Controlled, parametric, individualized, 2-D and 3-D imaging measurements of aerosol deposition in the respiratory tract of healthy human subjects for model validation. J Aerosol Sci 2012;52:1–17.

[8] Jackson AC, Gulesian Jr PJ, Mead J. Glottal aperture during panting with voluntary limitation of tidal volume. J Appl Physiol 1975;39:834–6.

[9] Baier H, Wanner A, Zarzecki S, Sackner MA. Relationships among glottis opening, respiratory flow, and upper airway resistance in humans. J Appl Physiol 1977;43:603–11.

[10] Brancatisano T, Collett PW, Engel LA. Respiratory movements of the vocal cords. J Appl Physiol 1983;54:1269–76.

[11] Chen Y, Maksym G, Brown T, Deng L. Determination of glottic opening fluctuation by a new method based on nasopharyngoscopy. Chin J Physiol 2013;56:52–7.

[12] Martonen TB, Zhang Z, Lessmann RC. Fluid dynamics of the human larynx and upper tracheobronchial airways. Aerosol Sci Technol 1993;19(2):133–56.

[13] Katz IM, Martonen TB, Flaa W. Three-dimensional computational study of inspiratory aerosol flow through the larynx: the effect of glottal aperture modulation. J Aerosol Sci 1997;28(6):1073–83.

[14] Katz IM, Davis BM, Martonen TB. A numerical study of particle motion within the human larynx and trachea. J Aerosol Sci 1999;30(2):173–83.

[15] Renotte C, Bouffioux V, Wilquem F. Numerical 3D analysis of oscillatory flow in the time-varying laryngeal channel. J Biomech 2000;33:1637–44.

[16] Gemci T, Shortall B, Allen GM, Corcoran TE, Chigier N. A CFD study of the throat during aerosol drug delivery using heliox and air. J Aerosol Sci 2003;34(9):1175–92.

[17] Brouns M, Jayaraju ST, Lacor C, De Mey J, Noppen M, Vincken W, et al. Tracheal stenosis: a flow dynamics study. J Appl Physiol 2007;102(3):1178–84.

[18] Brouns M, Verbanck S, Lacor C. Influence of glottic aperture on the tracheal flow. J Biomech 2007;40:165–72.

[19] Lin C-L, Tawhai MH, McLennan G, Hoffman EA. Characteristics of the turbulent laryngeal jet and its effect on airflow in the human intra-thoracic airways. Respir Physiol Neurobiol 2007;157(2-3):295–309.

[20] Xi J, Longest PW, Martonen TB. Effects of the laryngeal jet on nano- and microparticle transport and deposition in an approximate model of the upper tracheobronchial airways. J Appl Physiol 2008;104(6):1761–77.

[21] Heenan AF, Finlay WH, Grgic B, Pollard A, Burnell PKP. An investigation of the relationship between the flow field and regional deposition in realistic extra-thoracic airways. J Aerosol Sci 2004;35(8):1013–23.

[22] Henrich N. Mirroring the voice from Garcia to the present day: some insights into singing voice registers. Logoped Phoniatr Vocol 2006;31:3–14.

[23] Bailly L, Henrich N, Pelorson X. Vocal fold and ventricular fold vibration in period-doubling phonation: physiological description and aerodynamic modelings. J Acoust Soc Am 2010;127:3212–22.

[24] Childers DG, Naik JM, Larar JN, Krishnamurthy AK, Moore GP. Electroglottography, speech, and ultra-high speed cinematography. Vocal Fold Physiol Biomech Acoust Phonatory Control 1983:202–20.

[25] Švec JG, Šram F, Schutte HK. Videokymography: A new high-speed method for the examination of vocal-fold vibrations. Otorinolaryngol Foniatr 1999;48:155–62.

[26] Rothenberg M. A multichannel electroglottograph. J Voice 1992;6:36–43.

[27] Honda K, Maeda S. Glottal-opening and airflow pattern during production of voiceless fricatives: a new non-invasive instrumentation. J Acoust Soc Am 2008;123:3738.

[28] Ziethe A, Patel R, Kunduk M, Eysholdt U, Graf S. Clinical analysis methods of voice disorders. Curr Bioinforma 2011;6:270–85.

[29] England SJ, D, Bartlett J, Daubenspeck JA. Influence of human vocal cord movements on airflow and resistance during eupnea. J Appl Physiol 1982;52:773–9.

[30] Ghio A, Teston B. Evaluation of the acoustic and aerodynamic constraints of a pneumotachograph for speech and voice studies. Proc Int Conf Voice Physiol Biomech 2004:55–8.

[31] Juroszek B. Air features in spirometric transducers. Measurement 2006;39:466–76.

[32] Caselles V, Kimmel R, Sapiro G. Geodesic active contours. Int J Comput Vis 1997;22:61–79.

[33] Higenbottam T. Narrowing of glottis opening in humans associated with experimentally induced bronchoconstriction. J Appl Physiol 1980;49:403–7.

[34] Eckel HE, Sittel C. Morphometry of the larynx in horizontal sections. Am J Otolaryngol 1995;16:40–8.

[35] Hurbis CG, Schild JA. Laryngeal changes during exercise and exercise-induced asthma. Ann Otol Rhinol Laryngol 1991;100:34–7.

[36] Beaty MM, Wilson JS, Smith RJH. Laryngeal motion during exercise. The Laryngoscope 1999;109:136–9.

[37] Benchetrit G. Breathing pattern in humans: diversity and individuality. Respir Physiol 2000;122:123–9.

[38] Proctor DF, Hardy JB. Studies of respiratory air flow; significance of the normal pneumotachogram. Bull Johns Hopkins Hosp 1949;85:253–80.

[39] Hyatt RE, Wilcox RE. Extrathoracic airway resistance in man. J Appl Physiol 1961;16:326–30.

[40] D'Urzo AD, Rubinstein I, Lawson VG, Vassal KP, Rebuck AS, Slutsky AS, et al. Comparison of glottic areas measured by acoustic reflections vs. Comput Tomogr. J Appl Physiol Bethesda Md 1985 1988;64:367–70.

[41] Rubinstein I, England SJ, Zamel N, Hoffstein V. Glottic dimensions in healthy men and women. Respir Physiol 1989;77:291–9.

[42] Martin SE, Mathur R, Marshall I, Douglas NJ. The effect of age, sex, obesity and posture on upper airway size. Eur Respir J 1997;10:2087–90.

[43] Pritchard SE, McRobbie DW. Studies of the human oropharyngeal airspaces using magnetic resonance imaging. II. The use of three-dimensional gated MRI to determine the influence of mouthpiece diameter and resistance of inhalation devices on the oropharyngeal airspace geometry. J Aerosol Med Off J Int Soc Aerosols Med 2004;17:310–24.

[44] Kuna ST, Insalaco G, Villeponteaux RD. Arytenoideus muscle activity in normal adult humans during wakefulness and sleep. J Appl Physiol Bethesda Md 1985 1991;70:1655–64.

[45] Shiba K. Chapter 9.1 - Functions of larynx in breathing, vocalization and airway protective reflexes. Handb Behav Neurosci 2009:373–81.

[46] Hundertmark-Zaušková A, Lehmann R, Hess M, Müller F. Numerical simulation of glottal flow. Comput Biol Med 2013;43:2177–85.

[47] Templer JW, Von Doersten PG, Quigley PR, Scott GC, Davis WE. Laryngeal airway resistance: the relationships of airflow, pressure, and aperture. Arch Otolaryngol Neck Surg 1991;117:867–70.

[48] Idel'cik IE, Meury M. Mémento des pertes de charge coefficients de pertes de charge singulières et de pertes de charge par frottement. Paris: Eyrolles 1978.

[49] Jin HH, Fan JR, Zeng MJ, Cen KF. Large eddy simulation of inhaled particle deposition within the human upper respiratory tract. J Aerosol Sci 2007;38:257–68.